Journal of Physiology (1989), **415**, *pp.* 367–391
With 14 *text-figures*
Printed in Great Britain

CHARACTERISTICS OF VOLTAGE-GATED Ca^{2+} CURRENTS IN OVINE GONADOTROPHS

BY W. T. MASON AND S. K. SIKDAR

From the Department of Neuroendocrinology, AFRC Institute of Animal Physiology and Genetics Research, Babraham, Cambridge CB2 4AT

(*Received 5 August 1988*)

SUMMARY

1. Voltage-clamp recordings were obtained from gonadotrophs of the ovine pars tuberalis in dissociated cell culture, utilizing the whole-cell recording mode of the patch-clamp technique.

2. The amplitudes of Ca^{2+} and Ba^{2+} currents were dependent on the extracellular concentration of divalent cation.

3. Ba^{2+} tail currents were observed on termination of depolarizing voltage steps. The extrapolated amplitudes of 'instantaneous' tail currents increased with membrane depolarization and showed saturation beyond +15 mV.

4. True inactivation of currents occurred in the presence of both external Ca^{2+} and Ba^{2+}, judged from decrease in tail current amplitudes with progressive increases in duration of the activating voltage pulse. The inactivation process was fitted by a single-exponential function at membrane potentials below −25 mV, while at more depolarized potentials the inactivation was better described by a double-exponential function. The inactivation time constants decreased with positive shifts in membrane potential favouring a voltage-dependent inactivation.

5. The half-value of steady-state inactivation was observed at −40 mV using a two-pulse protocol.

6. Power spectral analysis of Ba^{2+} current noise from the steady-state portion of inward current showed a double Lorentzian fit of the power spectrum.

7. Two types of voltage-activated Ca^{2+} currents were identified based on their kinetics, voltage dependence, dependence on activation frequency, differential sensitivity to intracellular ATP and cyclic AMP, and to extracellular application of nifedipine. The channels with faster kinetics had a lower activation threshold (−50 mV) and the amplitude of the current was sensitive to clamping frequency.

8. From ensemble noise analysis of mean maximal inward current, single-channel amplitude of about 1 pA was estimated in 50 mM-Ba^{2+}.

INTRODUCTION

Secretion of LH (luteinizing hormone) and FSH (follicle stimulating hormone) by the pituitary gonadotrophs in response to the hypothalamic peptide gonadotrophin-releasing hormone (GnRH) is a Ca^{2+}-dependent process. Pharmacological manipu-

lations to affect permeability through Ca^{2+} channels influence gonadotrophin secretion in a positive or negative fashion (Conn, Rogers & Seay, 1983). At least part of this permeability occurs through voltage-activated Ca^{2+} channels, and their inherent kinetic properties will be expected to influence the amount of Ca^{2+} influx.

Most of our knowledge to date about the properties of voltage-gated calcium channels in anterior pituitary cells has been obtained from neoplastic cell lines (Hagiwara & Ohmori, 1982; Matteson & Armstrong, 1984), although work on isolated, characterized pituitary cells is beginning to emerge, mainly on lactotrophs and somatotrophs (Cobbett, Ingram & Mason, 1987; Mason & Rawlings, 1988). The main factor which has hampered work on gonadotroph electrophysiology has been the difficulty in obtaining a gonadotroph-rich cell population. The ovine pars tuberalis, however, contains gonadotrophs as the only hormone-secreting cell type (Gross, Turgeon & Waring, 1984), and electrophysiological studies on enzyme-dispersed and cultured gonadotrophs have revealed specific responses to GnRH (Mason & Waring, 1985, 1986) and the presence of voltage-activated ionic channels in these cells (Mason & Sikdar, 1988).

In the present report we describe some of the kinetic features of voltage-gated calcium channels in immunocytochemically identified ovine pars tuberalis gonadotrophs. Some preliminary aspects of the work have been presented to the Physiological Society and have appeared as an abstract (Mason, Sikdar & Waring, 1986).

METHODS

Cell culture

The ovine pars tuberalis was dissected under aseptic conditions from the brains of sheep obtained from a local abattoir. Gonadotrophs were isolated, dispersed and cultured as described previously by Mason & Waring (1985, 1986) and as utilized by Mason & Sikdar (1988).

Recording and data analysis

Recordings of calcium currents in gonadotrophs were made using whole-cell voltage-clamp techniques and data analysis identical to that recently described by Mason & Sikdar (1988) for sodium currents. The frequency response of the voltage clamp was 40 kHz, and the series resistances were in the range of 2–8 MΩ. Outside-out recordings were performed by pulling the electrode off the cell from the whole-cell recording configuration.

Solutions

Recordings were made from 3- to 15-day-old cultured cells. The culture medium was removed, rinsed 2–3 times with the recording solution, and finally substituted by 1 ml of the external recording solution. The culture dish was mounted on the stage of an inverted microscope with phase contrast optics (Leitz). Nifedipine was a gift from Bayer AG, Leverkusen, FRG. Nifedipine was dissolved in ethyl alcohol (EtOH), prepared and applied in the dark. Serial dilutions of the drug ensured a 1000-fold dilution of EtOH, to avoid any effect on the inward Ca^{2+} current.

For recording whole-cell currents the external solution had the following composition (in mM): Choline chloride, 105; $CaCl_2$ or $BaCl_2$, 25; TEACl, 10; HEPES, 5 and glucose, 10. For outside-out patch recordings the solution contained (in mM): $BaCl_2$, 100; and HEPES, 5. In experiments with 5 and 20 mM-Ba^{2+}, isotonicity was maintained by adjusting the choline chloride concentration. The patch pipette in both whole-cell and outside-out recordings was filled with solution containing (in mM): CsCl, 140; $CaCl_2$, 1; HEPES, 5; EGTA, 10; glucose, 10; Mg-ATP, 1; and cyclic AMP, 0·1.

RESULTS

The characteristics of Ca^{2+} channels in the gonadotrophs were mostly studied using Ba^{2+} in the external recording solution. This was for three reasons: (a) Ba^{2+} has a higher permeability than Ca^{2+} through Ca^{2+} channels (Hagiwara & Byerly, 1981; Hagiwara & Ohmori, 1982), (b) external Ba^{2+} suppresses certain types of outward currents carried by K^+ (Hagiwara, Miyazaki, Moody & Patlak, 1978), and (c) Ca^{2+}-dependent inactivation of Ca^{2+} channels is minimized in the presence of external Ba^{2+} (Eckert & Chad, 1984). A Cs^+-rich internal solution was used to suppress outward K^+ currents (Quandt & Narahashi, 1984). The presence of 10 mM-TEA (tetraethylammonium) in the external medium additionally ensured the suppression of outward currents through K^+ channels.

In preliminary experiments we confirmed a larger current amplitude in the presence of external Ba^{2+} than Ca^{2+}, and virtually similar inactivation characteristics of the current in the presence of either external Ba^{2+} or Ca^{2+}. No inactivation block or slowing of the current decay following activation was seen with Ba^{2+}, unlike some systems where inactivation is delayed in the presence of Ba^{2+}. Therefore, by examining the ionic current properties in Ba^{2+}, it was possible to extrapolate the findings to characteristics of Ca^{2+} flow through the same channels.

Dependence of inward currents on external Ba^{2+} concentrations

In the presence of either external Ba^{2+} or Ca^{2+}, gonadotrophs responded to depolarizing voltage pulses from a holding potential of -100 mV by producing inward currents. A membrane potential-dependent change in the current characteristics was seen. At less depolarized potentials (e.g. -30 mV in Fig. 1*A* and -35 mV in Fig. 7*A*), current activation was followed by inactivation almost to the zero current level. At more depolarized potentials, however, a rapid activation step was followed by much slower inactivation of the current to a sustained steady-state level.

The influence of two different Ba^{2+} concentrations upon inward currents are illustrated in Fig. 1. The amplitudes of both peak and steady-state currents were concentration dependent, and the amplitude of maximal inward current increased with Ba^{2+} concentration (Fig. 1*A* and *B*). At concentrations greater than 20 mM, there was a rightward shift in the maximal peak activation of the Ba^{2+} current along the voltage axis.

Tail currents

Voltage activation of the cells to depolarized potentials produced a tail current at the end of the pulse due to a sudden change in the driving force, indicated by arrows in Fig. 2*A*. The kinetics of tail current decays were analysed by fitting exponential functions and were best fitted by a double-exponential function of the form:

$$I_t = I' \exp(-t/\tau_1) + I'' \exp(-t/\tau_2),$$

where I' and I'' are current amplitudes, t is time, and τ_1 and τ_2 are time constants of fast and slow processes respectively.

The tail current amplitudes were analysed by extrapolating the tail current decline

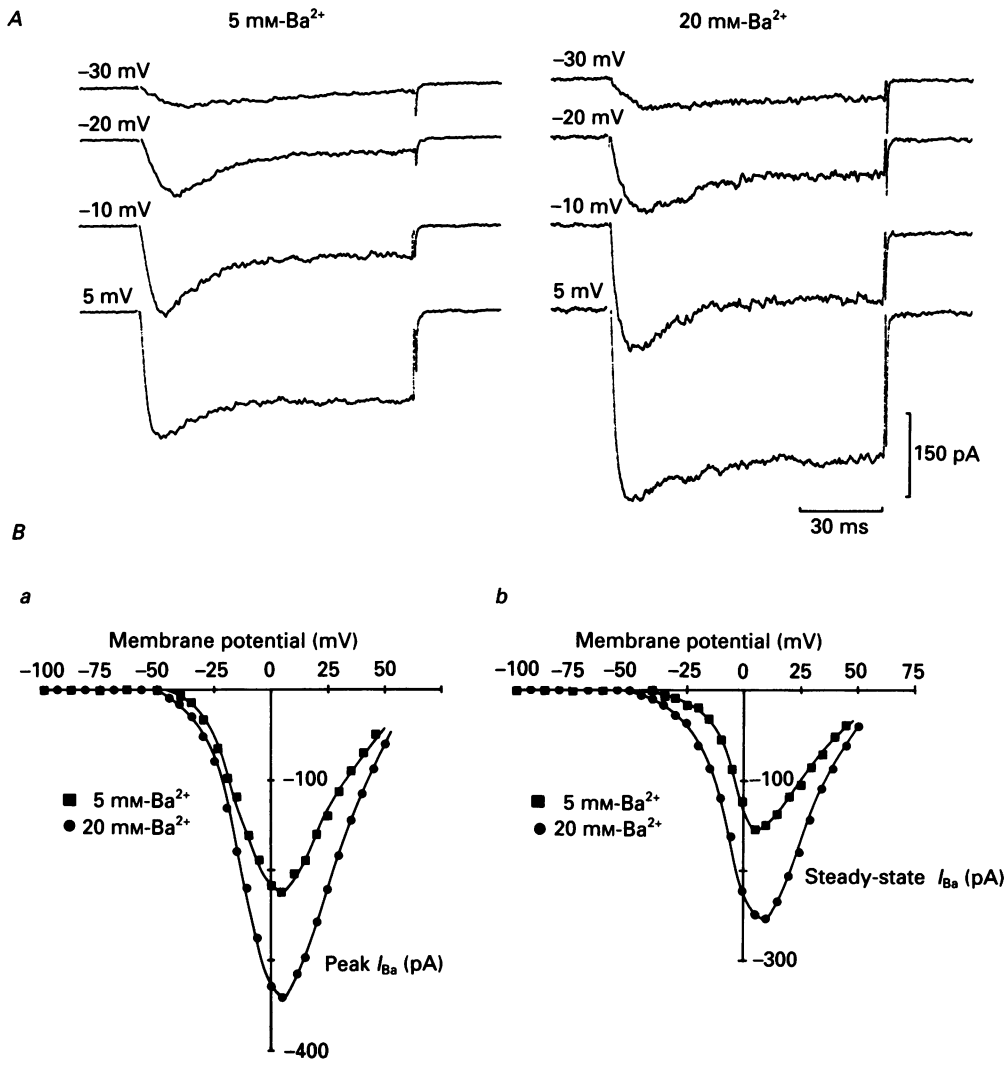

Fig. 1. Effects of 5 and 20 mM-Ba^{2+} on clamp currents. *A*, averaged inward current records ($n = 5$) in the presence of external Ba^{2+} concentration 5 (*a*) and 20 mM (*b*) at the membrane potentials indicated on the left of traces. Holding potential, −100 mV. *B*, *I–V* relationship for the peak and steady-state inward currents in 5 and 20 mM-external Ba^{2+}. All records are from the same cell.

to the end of the test pulse. Figure 2*B* shows a plot of the tail current amplitudes at different test potentials along with a plot of the peak and steady-state current. The time constants of the two components of the tail current decays were essentially similar at different test potentials. The plot of tail current amplitude *versus* membrane potential showed saturation at potentials above +20 mV. Since the tail current amplitude is proportional to the fraction of channels activated at a particular membrane potential, the hump in the curve seen at around −10 mV might reflect a change in the activation properties of the channel in question, or the region where additional contributions from a different population of channels occur. The plot is also

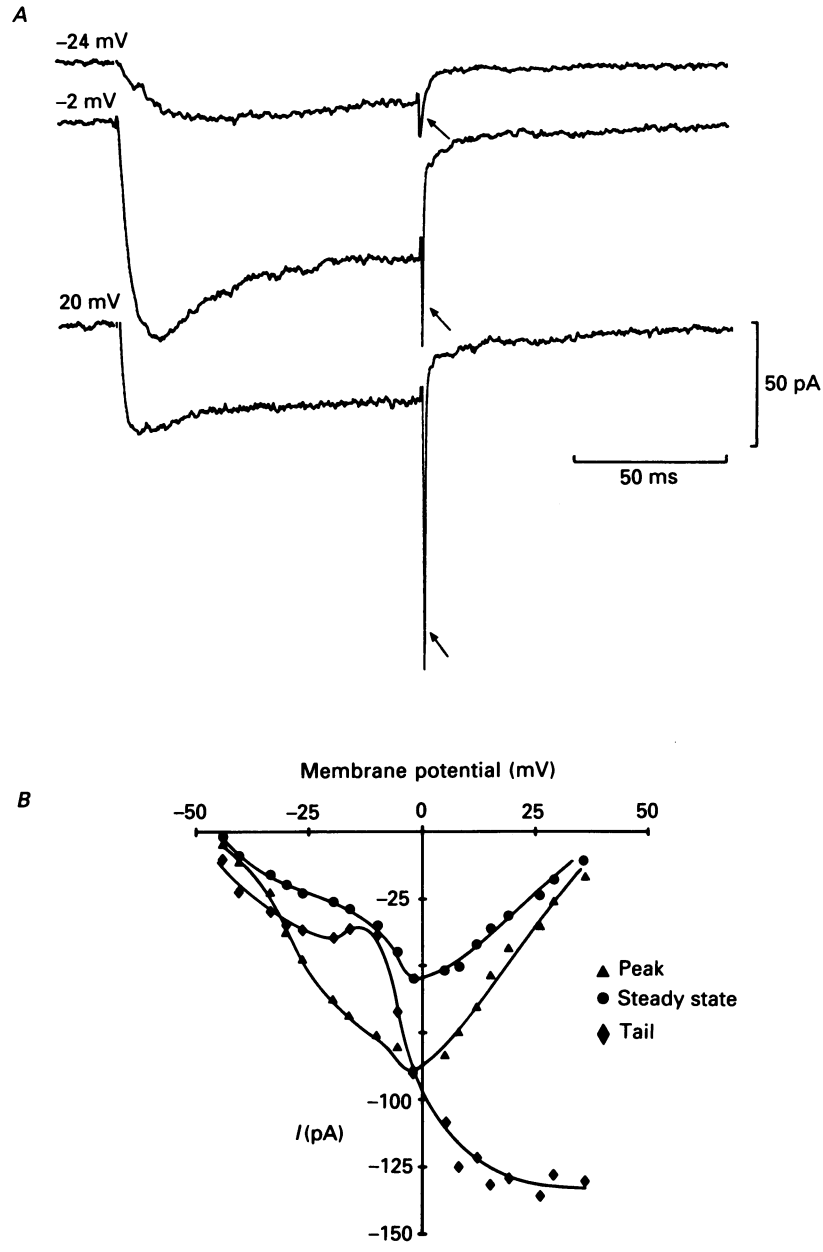

Fig. 2. Voltage activated currents in 25 mM-Ba^{2+}. *A*, samples of averaged current records, leakage and capacitance subtracted, produced by 100 ms pulses to membrane potentials indicated on the left of the traces. Holding potential, −100 mV. Note the fast and the slow inactivating component in the current records followed by the tail currents (indicated by slanted arrows) at the termination of the voltage pulse. The tail current showed a progressive increase in amplitude with increase in the amplitude of the depolarization step. *B*, plot of peak, steady-state and tail current amplitudes as a function of membrane potential.

sigmoidal, with saturation of the current occurring beyond 5 mV. The general trend resembles the tail current–voltage characteristics described in the squid giant axon synapse (Llinás, Steinberg & Walton, 1981), bovine chromaffin cells (Fenwick, Marty & Neher, 1982) and GH3 cells (Hagiwara & Ohmori, 1982). This saturation indicates maximal opening of the channels permeable to calcium, and therefore, maximal conductance.

Activation of Ba^{2+} current

In the absence of contamination of the Ca^{2+}/Ba^{2+} current by other ions, it was possible to analyse the kinetics of the activation phase of the current, after subtraction for leakage and capacitive transients. The activation phase of the current was analysed according to the model of Hodgkin & Huxley (1952), by assuming that the current could be described by $i_{Ba} = I_{Ba}m^y h$, where h is the inactivation parameter. To determine the appropriate value of the exponent y of the activation parameter m, the equation $1-[I(t)/I(\infty)]^{1/y}$ was plotted against time, t, on a semilogarithmic scale (Belluzzi, Sacchi & Wanke, 1985), where $I(t)$ is current at time t. The value of $y = 1$ best fitted the experimental points. This is shown for depolarizations to 0 and -10 mV in the same cell (Fig. 3*A*).

Another method was employed (Kostyuk, Veselovsky & Fedulova, 1981) to analyse the activation phase of the currents in the same cells, which involved plotting the current amplitude *versus* time on a double logarithmic scale. This is shown for currents at four different depolarization potentials (Fig. 3*B*). The exponent y, of m, is determined from the tangent of the straight line slope, or by performing linear regression analysis on the natural logarithms of current and time and determing the slope factor. Estimations of the value of the exponent y from these procedures yielded values of 0·76, 0·95, 1·0 and 0·9 for depolarizations of the cell to 0, -10, -20 and -30 mV respectively. From these analyses, the appropriate value of the exponent was concluded to be 1 (three cells). For the cell shown in Fig. 3, the time constant of activation was found to decrease from 2·7 ms at -10 mV to 1·9 ms at 0 mV. This was determined from the relationship,

$$\ln \{1-[I(t)/I(\infty)]^{1/y}\} = -t/\tau,$$

where $I(t)$ is current at time t, and τ is the time constant of activation.

Different values of y, ranging from 1 to 6, have been determined for other cells (see Hagiwara & Byerly, 1981). The value of $y = 1$ for Ca^{2+} current in gonadotrophs corroborates with a similar value determined in tunicate egg (Okamoto, Takahashi & Yoshii, 1976) and Helix neurone (Akaike, Lee & Brown, 1978).

Instantaneous I–V relationship

A macroscopic approach to understand the voltage dependence of single-channel behaviour is to activate the channels to produce maximal conductance and thence to measure the amplitude of the current produced at the end of the pulse (tail) at different repolarization potentials. This can be explained by considering the following general equation which summarizes the factors influencing the macroscopic current through a single class of channels:

$$I = gNF(V_m - E),$$

where I = macroscopic current amplitude in external Ca^{2+}/Ba^{2+}, g = single-channel conductance incorporating permeability and selectivity properties of the channel, N = number of channels, $V_m - E$ = driving force, V_m = membrane potential, E = reversal/equilibrium potential for Ca^{2+}/Ba^{2+}, and F = fraction of activated channels.

In the two-pulse protocol mentioned above, the change in g during the second

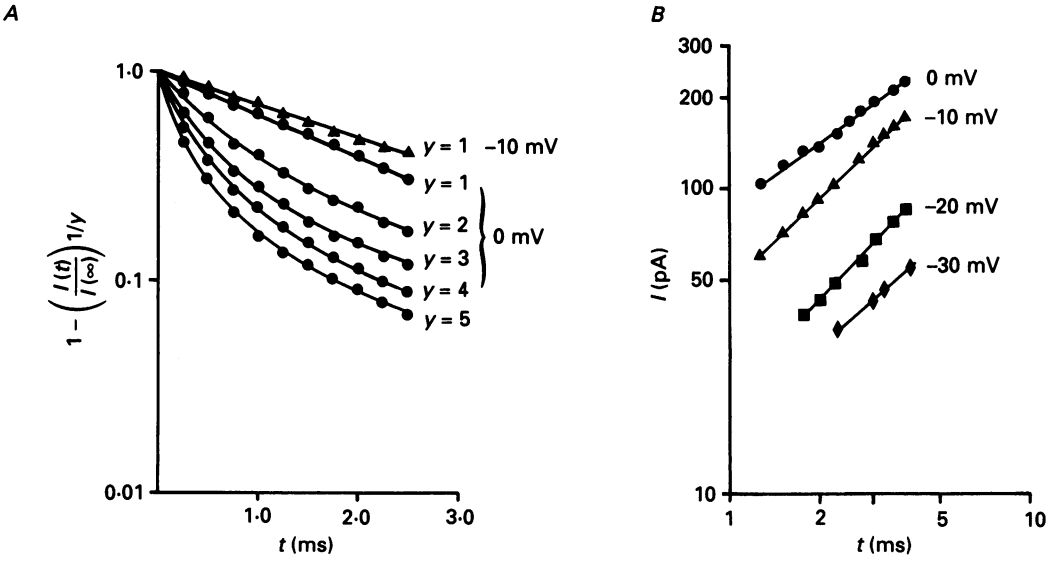

Fig. 3. Activation of Ba^{2+} current. *A*, the current amplitude is plotted against time according to the eqn $\ln\{1-[I(t)/I(\infty)]^{1/y}\} = -t/\tau$, where I is current amplitude, and t is time. Values of y = 1–5 were used. A straight line was best fitted with $y = 1$, shown in the figure for currents evoked by voltage pulse to −10 and 0 mV. *B*, a double logarithmic plot of current amplitude against time for I_{Ba} produced by potential steps to levels indicated on the right side of the straight line slopes. Same cell as in *A*. The tangent of the straight line slope (see text) determined the exponent y for activation variable. Filter frequency, 2 kHz; digitizing frequency, 4 kHz.

pulse is instantaneous, while the change in F takes a relatively longer time, thus making it possible to separate the influence of voltage on g from F. With the number (N) and the fraction of activated channels (F) remaining constant throughout maximal activation of the current during the first pulse, the changes in tail current amplitude with the repolarization potential can be attributed solely to changes in potential-dependent conductance of single channels.

Tail currents which were obtained following a 7 ms depolarizing pre-pulse to 10 mV from a holding potential of −100 mV, followed immediately by a repolarizing post-pulse to different membrane potentials, are shown in Fig. 4*A*. Repolarizing the membrane to depolarized membrane potentials reduced the amplitude of the tail current. A plot of the tail current amplitudes against the repolarization potentials gave the instantaneous *I–V* relationship, illustrated by the plot in Fig. 4*B*. The tail current amplitude measurements used for the plot, were obtained after leakage and capacitive subtraction.

The following constant field equation was used at first to fit the instantaneous I–V relationship:

$$I_{Ba} = P_{Ba}\frac{4VF^2\{[Ba^{2+}]_i(\exp 2VF/RT)-[Ba^{2+}]_o\}}{\exp(2VF/RT)-1},$$

where I_{Ba} is the membrane current; P_{Ba} is the permeability coefficient; $[Ba^{2+}]_i$ is the internal Ba^{2+} concentration which was assumed to be the same as that of Ca^{2+} (10^{-8} M); $[Ba^{2+}]_o$ is the external Ba^{2+} concentration, 25 mM; R, T and F are gas constant, absolute temperature and Faraday's constant respectively; and V is the membrane potential. The actual units of $[Ba^{2+}]_i$ and $[Ba^{2+}]_o$ used were mol/cm^3, and since I_{Ba} had the unit of ampere rather than ampere/cm^2, P_{Ba} has the unit of cm^3/s. For a proper fit it was necessary to vary the value of P_{Ba} from 10^{-11} to 10^{-12} cm^3/s over the complete voltage range, the higher values of P_{Ba} corresponding to the less negative repolarization potentials. A modified form of constant field equation (see Brown, Tsuda & Wilson, 1983) gave a much better fit:

$$I_{Ba} = P(V-V')\frac{\{[Ba^{2+}]_o\exp(-2V'/H)\}}{1-\exp[2(V-V')/H]},$$

where P, H and V' are constants. The values of the constants derived from the fit of instantaneous I–V relation shown in Fig. 4 were, $V' = 75{\cdot}2$ mV, $H = 16{\cdot}7$ mV and $P = 442$ pA/(mV mM). A non-linear instantaneous I–V has been reported earlier in rat anterior pituitary tumour cells (Dubinsky & Oxford, 1984). The basic nature of the instantaneous I–V relationship was not affected by using a pre-pulse of long duration.

Inactivation of Ba^{2+} current

Following the activation of the current with Ca^{2+} or Ba^{2+} as the charge carrier and internal Cs^+, the current declined in amplitude with time. To ascertain whether this decline was due to current decay and not to simultaneous activation of an outward current, we used the tail current method. The procedure involved the observation of tail current amplitude, following pulses of varying duration. In the example illustrated in Fig. 5, it can be seen that the amplitude of tail current becomes shorter with increase in pulse duration.

Voltage dependence of inactivation

The measurement for the steady-state inactivation ($h(\infty)$–V) plot using the two-pulse protocol, require pre-pulses of long duration to reach the steady state. With Ca^{2+} or Ba^{2+} currents, however, this can only be achieved using very long pre-pulse durations (2–10 s), which limits the number of repetitions possible, and may adversely affect the cell. Varying the holding potential with a constant test-pulse amplitude proved equally difficult. We therefore, used pre-pulses of short duration (100 ms). However, this affected the measurements since the inactivation process initiated by the pre-pulse was not complete.

In the experiment illustrated in Fig. 6*A*, a double-pulse protocol was used to examine the inactivation process. The amplitude of the current in response to a 100 ms duration test pulse to +10 mV varied with the pre-pulse amplitude. The amount

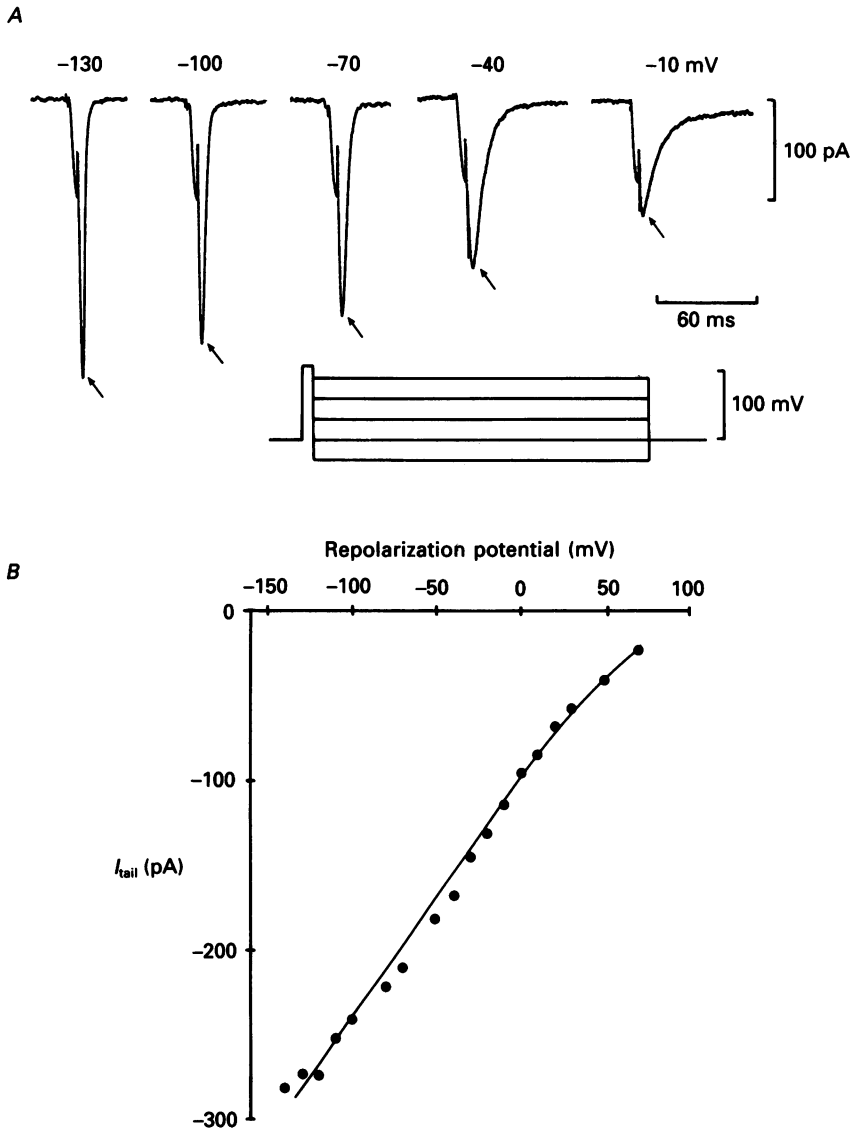

Fig. 4. Instantaneous *I–V* relationship in 25 mM-external Ba^{2+}, using a two-pulse protocol with a short pre-pulse (7 ms) to +10 mV, followed by repolarization to different membrane potentials. Holding potential, −100 mV. Averaged ($n = 5$) pre-pulse and tail current records (indicated by arrows) leak and capacitance subtracted. Repolarization potentials are indicated above the traces (mV). *B*, plot of tail current amplitudes against repolarization potentials. The line through the data points represents the fit with the equation described in the text. A non-linear regression analysis on the fit gave $R^2 = 0{\cdot}99$, which indicates what proportion of the sum of squares about the mean of the raw Ba^{2+} tail current values is accounted for by the deviation of the fitted model about mean.

of inactivation left by the pre-pulse was a smooth function of the pre-pulse, resulting in a sigmoidal $h(\infty)$–V plot. The sigmoidal $h(\infty)$–V curve was fitted by,

$$h(\infty) = 1/\{1+\exp[(V-V_{\frac{1}{2}})/4{\cdot}9]\},$$

where V is the membrane potential, and $V_{\frac{1}{2}}$ is the potential at half-maximal inactivation, i.e. $h(\infty) = 0{\cdot}5$.

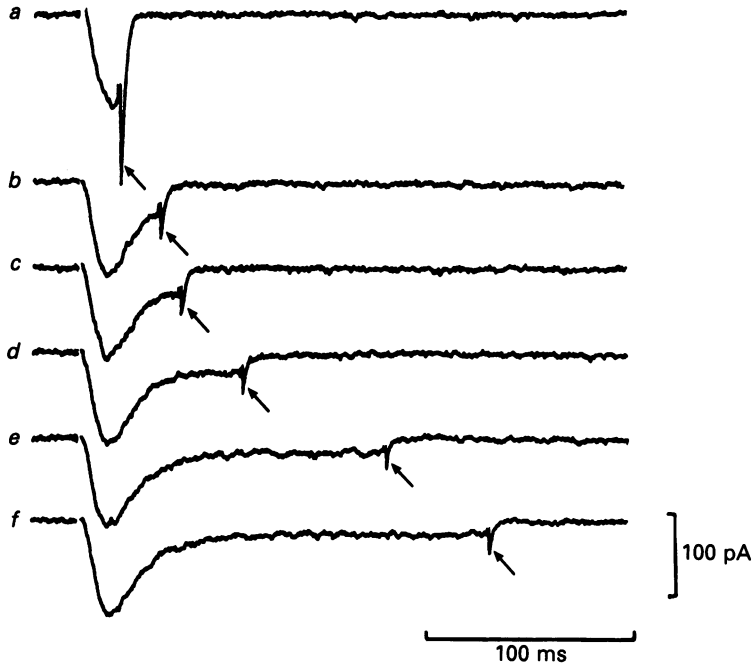

Fig. 5. Tail currents at different pulse durations. Inward currents were elicited by depolarizing the membrane to −20 mV from a holding potential of −100 mV at progressively increasing pulse durations (*a–f*). The tail currents at the end of the pulse are indicated by arrows. Note the initial rapid followed by a slow decline of the tail current amplitude.

The amount of inactivation increased with the pre-pulse potential, with half-inactivation ($V_{\frac{1}{2}}$) occurring at around −40 mV, and the currents remained inactivated even with more positive shifts in the pre-pulse potential. This observation is indicative of a voltage-dependent inactivation of the current (Fox, 1981) rather than a Ca^{2+}-dependent process (Mentrad, Vassort & Fischmeister, 1984) or a mixed Ca^{2+}- and voltage-dependent process, where the inactivation decreases as the pre-pulse potential approaches the reversal potential for Ca^{2+} or Ba^{2+}, resulting in a U-shaped $h(\infty)$–V curve (Hadley & Hume, 1987).

Voltage dependence of inactivation time constant

The inactivation phase of the currents were fitted either by a single- or a double-exponential function. At less depolarized test potentials (−35 to −5 mV) the inactivation phase decayed to the zero current level, and was fitted by a single-exponential function. At more depolarized test potentials however, the inactivation

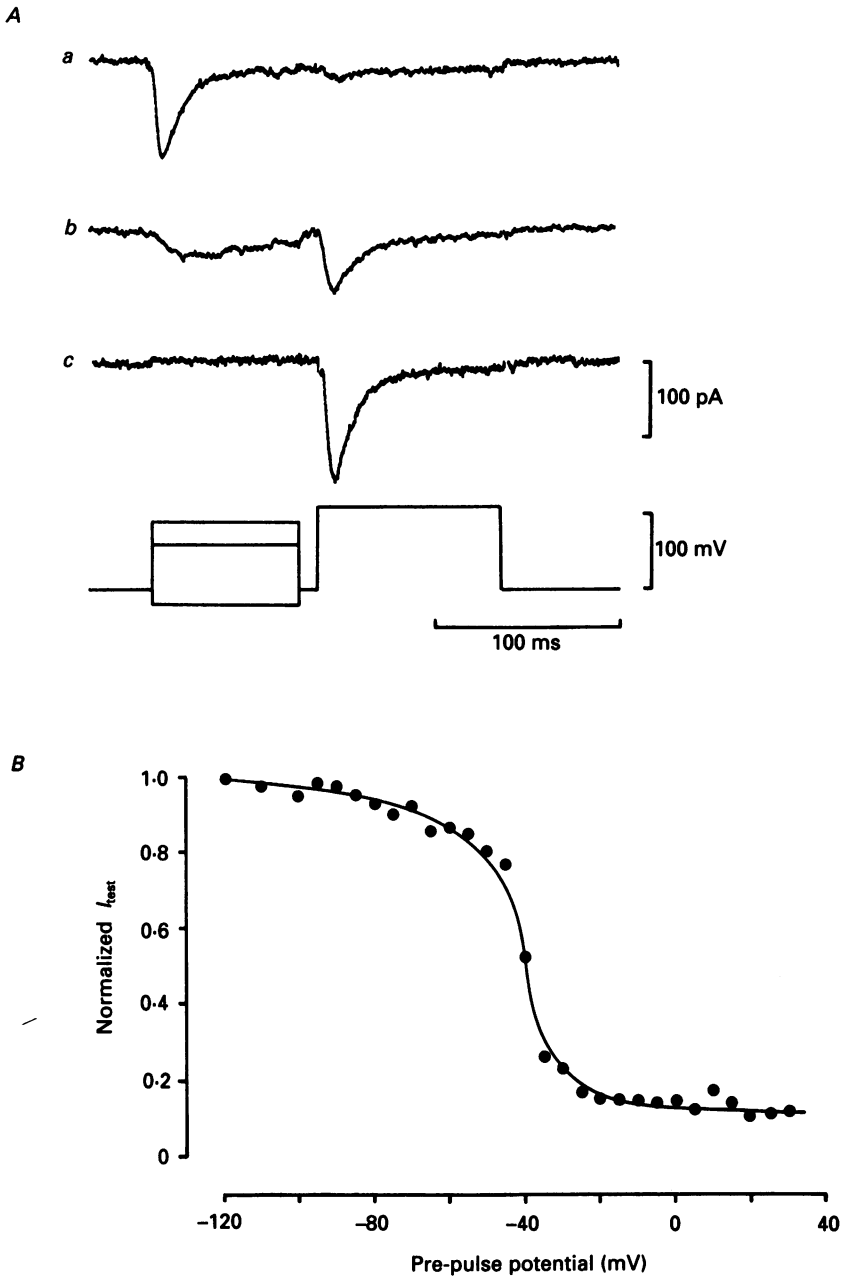

Fig. 6. Steady-state inactivation of Ba^{2+} current. *A*, current records obtained using a two-pulse protocol consisting of variable amplitudes of depolarizing and hyperpolarizing pre-pulses and a constant test-pulse to +10 mV separated by a gap of 10 ms. Test-current amplitudes at three different pre-pulse potentials are shown. *B*, steady-state inactivation of Ba^{2+} current obtained by plotting the normalized fraction of Ba^{2+} current (peak) as a function of the pre-pulse potential.

phase showed an additional slowly declining component and was fitted by a double-exponential function (Fig. 7*A*). The inactivation kinetics were judged to be voltage dependent, given the relationship of the time constant of the fast component (τ_1) with membrane potential (shown in Fig. 7*B*).

Fluctuation analysis of Ba^{2+} currents

The underlying microscopic fluctuations in the membrane current as a basis of the voltage-activated macroscopic currents were evident on subtracting an individual

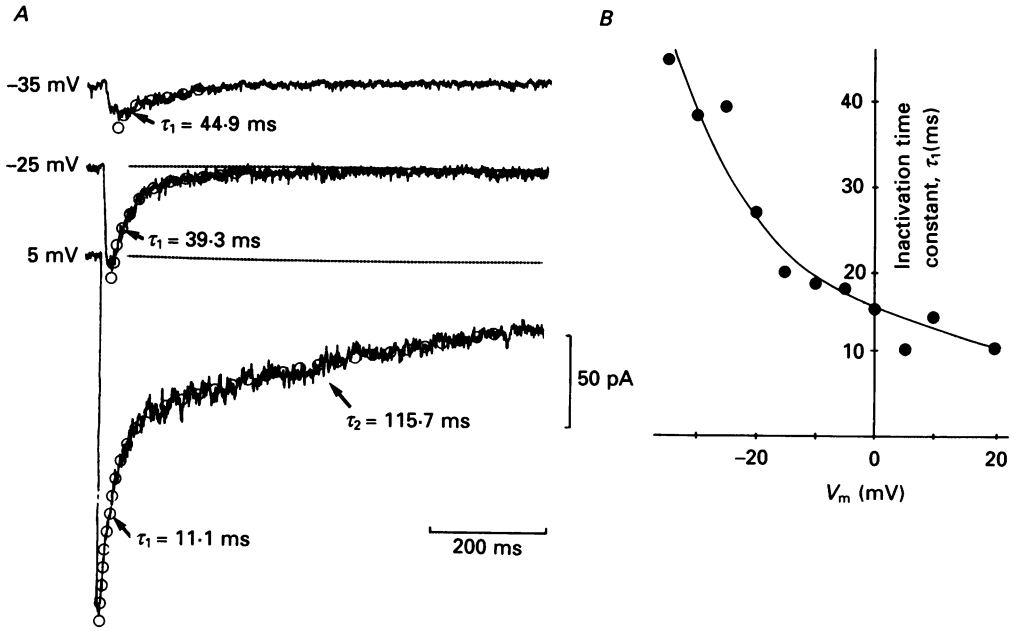

Fig. 7. Voltage dependence of inactivation time constant of Ba^{2+} current. *A*, averaged Ba^{2+} current records showing the inactivation phases of the inward currents along with the inactivation time constants determined from the best exponential fits, at the membrane potentials indicated on the left of the traces. The inactivation phases of the currents at less depolarized potentials was best fitted by a single-exponential function while at more depolarized potentials (0 mV and above) by a double-exponential function. *B*, plot of inactivation time constant of the fast component (τ_1) as a function of membrane potential. The relationship indicates voltage dependence of the inactivation time constant. Filter frequency, 2 kHz, digitizing frequency, 4 kHz.

Ba^{2+} current trace from the average Ba^{2+} current record. The amplitude of current fluctuations during the duration of voltage pulse were larger than the baseline fluctuations.

We analysed the kinetics of the microscopic current fluctuations by obtaining a power density spectrum of the Ba^{2+} current fluctuations from the steady-state portion of the Ba^{2+} inward current record. The membrane current fluctuations at two different potentials of -20 and -5 mV derived from their respective steady-state portion of the Ba^{2+} current records are illustrated in Fig. 8. The amplitude of the membrane current fluctuations at -5 mV (Fig. 8*B*) was larger than at -20 mV (Fig. 8*A*). This was also evident from the magnitude of the zero frequency asymptote of the power density spectral plot.

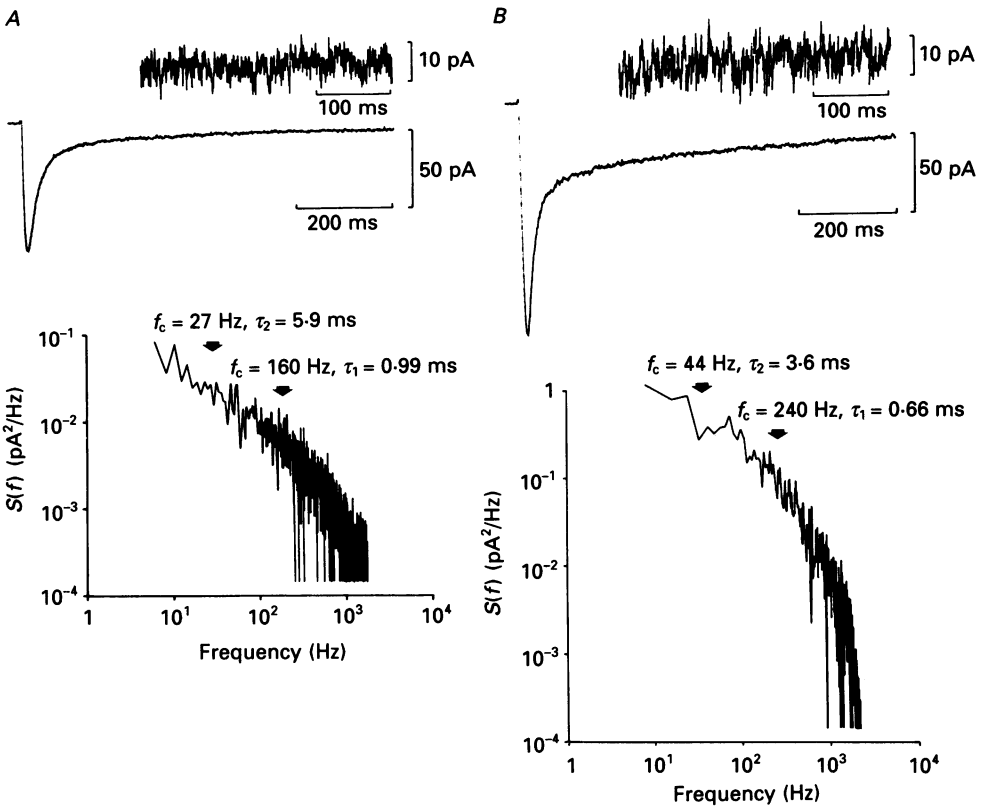

Fig. 8. Power density spectra of Ba^{2+} currents at −20 (*A*) and −5 mV (*B*) in 50 mM-external Ba^{2+}. Holding potential, −100 mV. The traces in the upper right-hand corner show a sample of the current fluctuations (upper trace) derived from the steady-state portion of the Ba^{2+} inward currents (lower trace) obtained using a pulse of 1 s duration. The power spectral density was fitted by a double Lorentzian function. The arrows indicate the cut-off frequency points (f_c) from which the time constant values (τ_1 and τ_2) were derived using the equation described in the text. Note the decrease in time constant values of the slow and fast components at a more depolarized potential (−5 mV, *B*) than at a less depolarized potential of −20 mV (*A*). *A* and *B* are from the same cell. Filter frequency, 2 kHz; digitizing frequency, 4 kHz; Butterworth filter.

The time constant values estimated from the double Lorentzian fit of the power density spectrum and the differences in the time constant values estimated at the two different potentials (τ_1 = 0·99 and τ_2 = 5·9 ms at −20 mV; τ_1 = 0·66 and τ_2 = 3·6 ms at −5 mV) are indicative of the fact that the time constants of both underlying kinetic processes are voltage dependent. The double Lorentzian fit is also suggestive of two types of membrane calcium channels, each with different kinetic parameters.

Comparison of τ_1 and τ_2 values obtained from analyses of activation kinetics, tail current decay and power spectra

In order to understand whether the kinetics of the two components of calcium current identified by using three different analytical procedures (activation of the calcium current, noise-power spectra and tail current decays) were similar, we

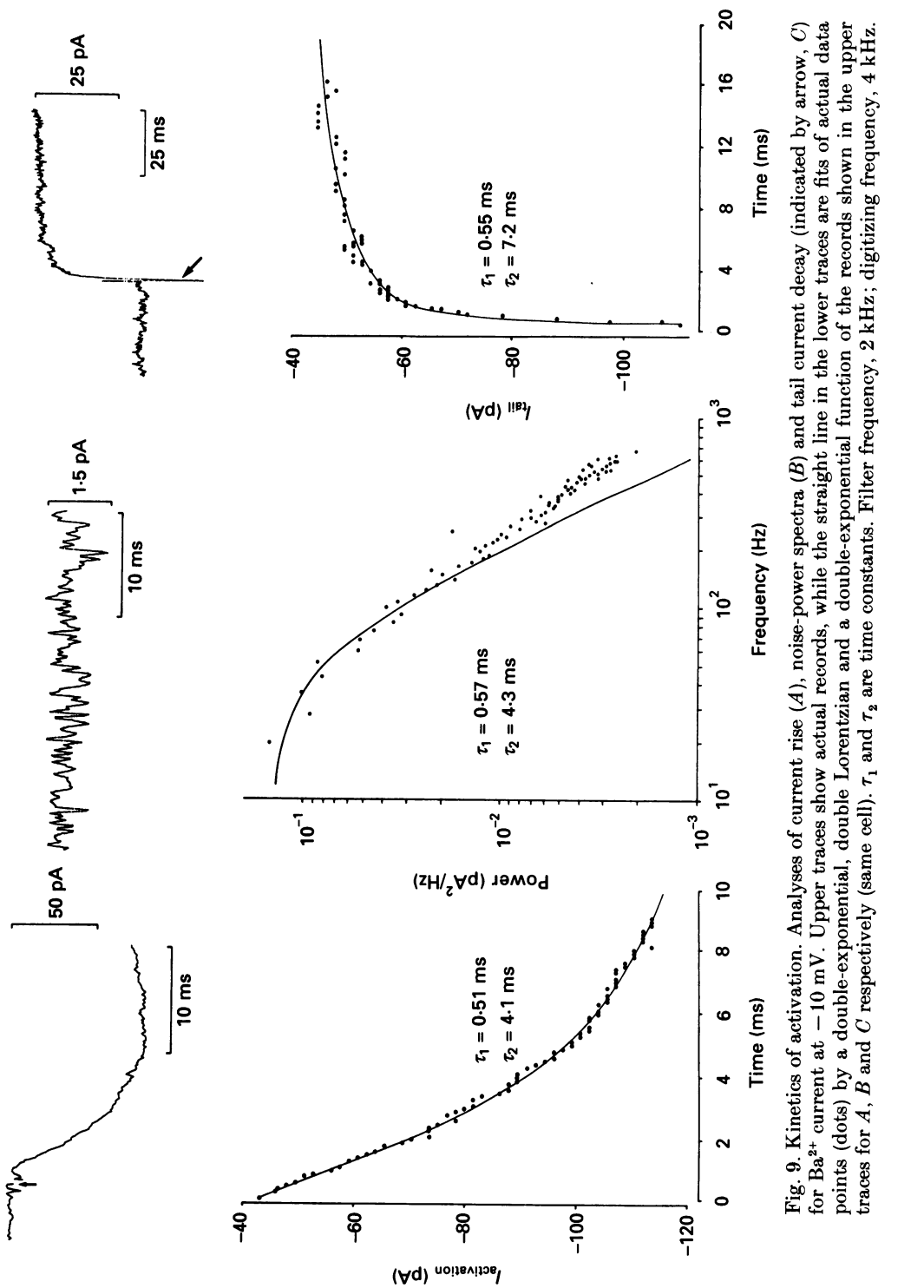

Fig. 9. Kinetics of activation. Analyses of current rise (*A*), noise-power spectra (*B*) and tail current decay (indicated by arrow, *C*) for Ba^{2+} current at −10 mV. Upper traces show actual records, while the straight line in the lower traces are fits of actual data points (dots) by a double-exponential, double Lorentzian and a double-exponential function of the records shown in the upper traces for *A*, *B* and *C* respectively (same cell). τ_1 and τ_2 are time constants. Filter frequency, 2 kHz; digitizing frequency, 4 kHz.

analysed the kinetics of the two components in the same cell, using all the three procedures. As illustrated in Fig. 9, for a Ba^{2+} current evoked at -10 mV, near identical τ_1 and τ_2 values were obtained from a double-exponential fit of the activation phase (*A*) and tail current decay (*C*) and a double Lorentzian fit of the noise-power spectrum (*B*). The following relation was used for the double Lorentzian fit, viz.

$$S(f) = S(0)/\{[1+(2\pi f\tau_1)^2]+[1+(2\pi f\tau_2)^2]\},$$

where $S(0)$ is spectral density at zero frequency; f, frequency in hertz, τ_1 and τ_2 are time constants (see Mason & Sikdar, 1988). From this it is possible to conclude that voltage-dependent activation of calcium current involves activation of two different channel types with different kinetics. Similar τ_1 and τ_2 values derived from the three different analytical procedures concur with observations of Fenwick, Marty & Neher (1982) in bovine chromaffin cells.

Two different activation thresholds for Ba^{2+} currents

Figure 10 shows the difference in Ba^{2+} current records observed at two different holding potentials. When the membrane was held at -100 mV, depolarized voltage steps elicited currents which showed both rapid and slow inactivating components (*A a*). On the other hand, when the membrane potential was held at -50 mV, similar depolarizing voltage steps did not activate the fast inactivating current, although the slow inactivating component was similar to that obtained at a holding potential of -100 mV. While the rate of inactivation of the current was much greater when the holding potential was at -100 mV, the amplitude of the residual current at the end of the pulse was identical at both holding potentials.

Figure 10*B* shows the voltage dependence of the peak Ca^{2+} current at two different holding potentials. On subtracting the *I–V* relationship obtained at a holding potential of -50 mV from that at -100 mV, a rough estimate of the voltage dependence of the fast inactivating component could be made since the currents using voltage pulses for a holding potential of -100 mV contained a mixture of both fast and slow inactivating components, while at -50 mV the currents primarily consisted of the slow inactivating component. The differences in the activation threshold and maximal peak activation of the two different components became apparent from this plot. Maximal peak activation of the low threshold, fast-inactivating current occurred at -30 mV, while for the slow inactivating current, maximal peak activation was observed at -10 mV.

Differential sensitivity to activation frequency of the two components

A repetitive stimulus protocol was used to examine the differential sensitivity of the two components of the Ca^{2+}/Ba^{2+} currents. Figure 11*A* shows the current characteristics at pulse numbers 1, 8 and 13 of a pulse train evoked in 25 mM-Ca^{2+} at frequencies of 0·2, 2 and 4 Hz. Note the decline in the amplitude of the fast component of the currents at higher pulse numbers with increase in the pulse frequency, and a near constant amplitude of the slow decaying component of the current.

The frequency dependence of the fast component is shown in a plot of the non-inactivated fraction of Ca^{2+} current *versus* pulse number at different frequencies. The

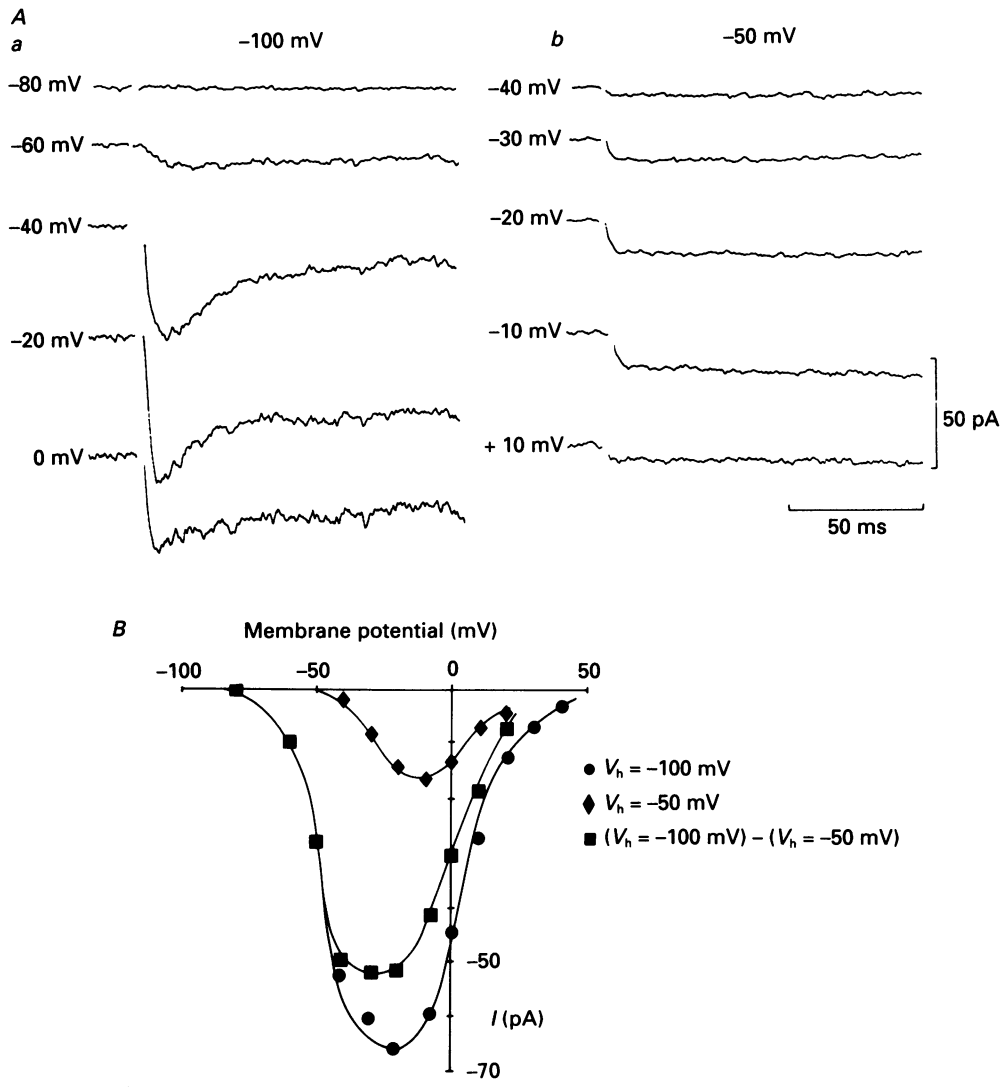

Fig. 10. Comparison of Ca^{2+} current records produced by using depolarizing voltage steps from two different holding potentials. *A*, averaged Ca^{2+} current records ($n = 5$) to membrane potentials indicated on the left of the current traces, from a holding potential (V_h) of -100 mV (*a*) and -50 mV (*b*). *B*, *I–V* relationship for peak Ca^{2+} currents from two different holding potentials, and plot of *I–V* relationship of the fast component by a subtraction procedure (peak current at $V_h = -100$ mV $-$ peak current at $V_h = -50$ mV).

slow recovery from inactivation of the fast component is depicted in Fig. 11*C*. Here, the steady-state value of the non-inactivated fraction of Ca^{2+} current obtained from Fig. 11*B* is plotted against the time spent at the holding potential (V_h), derived from the interpulse interval stimulation frequency.

Effects of nifedipine

In addition to the electrophysiological distinction between the two Ca^{2+} channel types, a difference in pharmacological sensitivity was also evident. Figure 12 shows

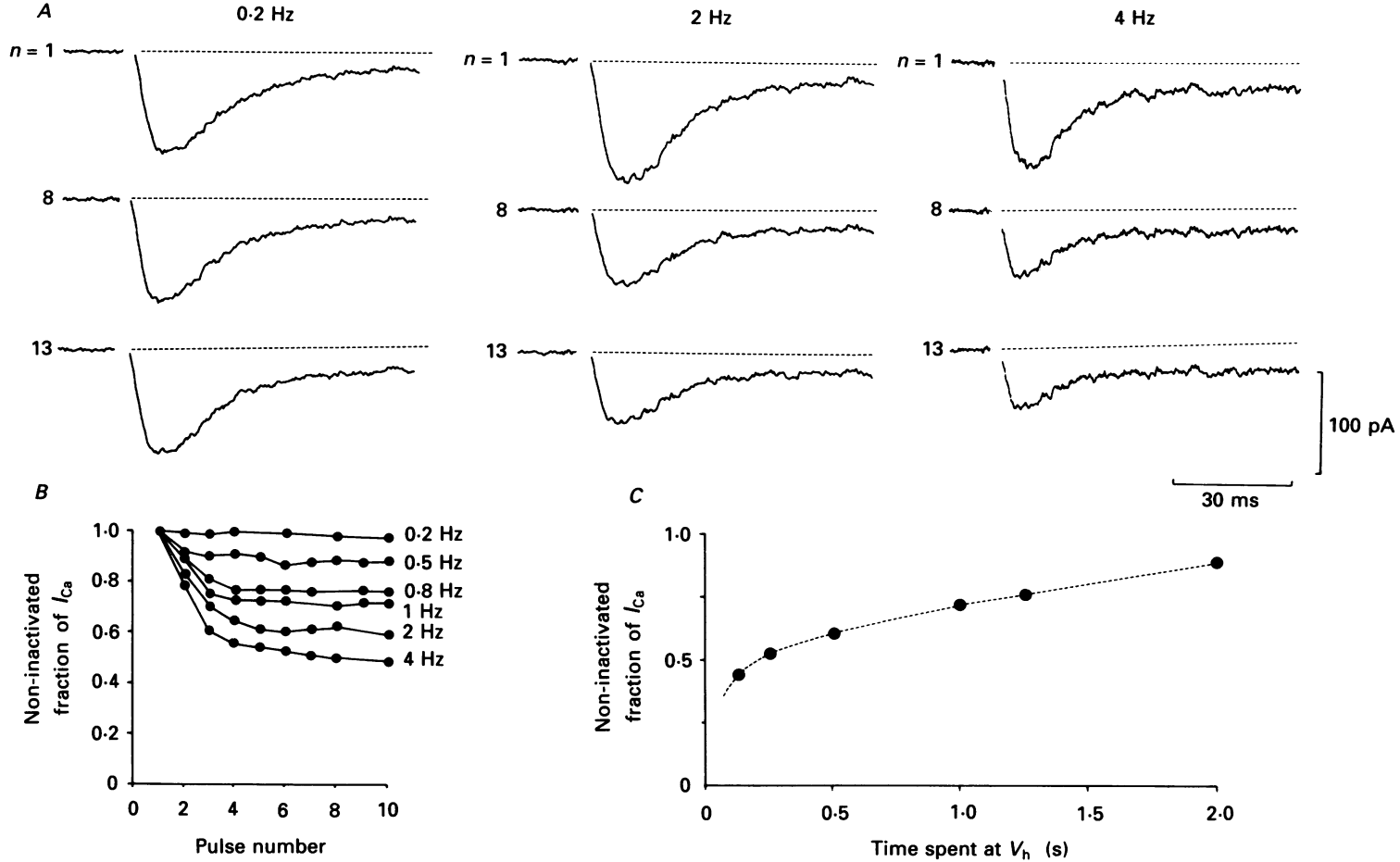

Fig. 11. Dependence of Ca^{2+} current on frequency, and recovery from inactivation. The figure shows Ca^{2+} current records at three different clamp frequencies to show the effect of frequency on the magnitude of the fast and slow inactivating currents. Holding potential (V_h), −100 mV; test potential, −20 mV; pulse duration, 100 ms. The numbers on the left of the current traces refer to the pulse number (n) in the train. Increasing the frequency attenuated the fast inactivating component of the Ca^{2+} current. *B*, plot of the normalized fraction of the peak current against pulse number at different clamp frequencies indicated on the right. *C*, plot of the normalized peak current amplitude at the equilibrated state obtained from the plot in *B*, against the interpulse interval, i.e. time spent at V_h. Note the slow recovery from inactivation of the current.

the effects of 10 μM-nifedipine, a dihydropyridine Ca^{2+} channel blocker, on a cell which showed both a fast and slow inactivating component (control, Fig. 12*A*) to depolarizing voltage steps in 25 mM-external Ca^{2+}. Nifedipine (10 μM) predominantly affected the slow inactivating component by attenuating it. At potentials where the slow inactivating component was blocked, the fast inactivating component was not affected (Fig. 12*B*).

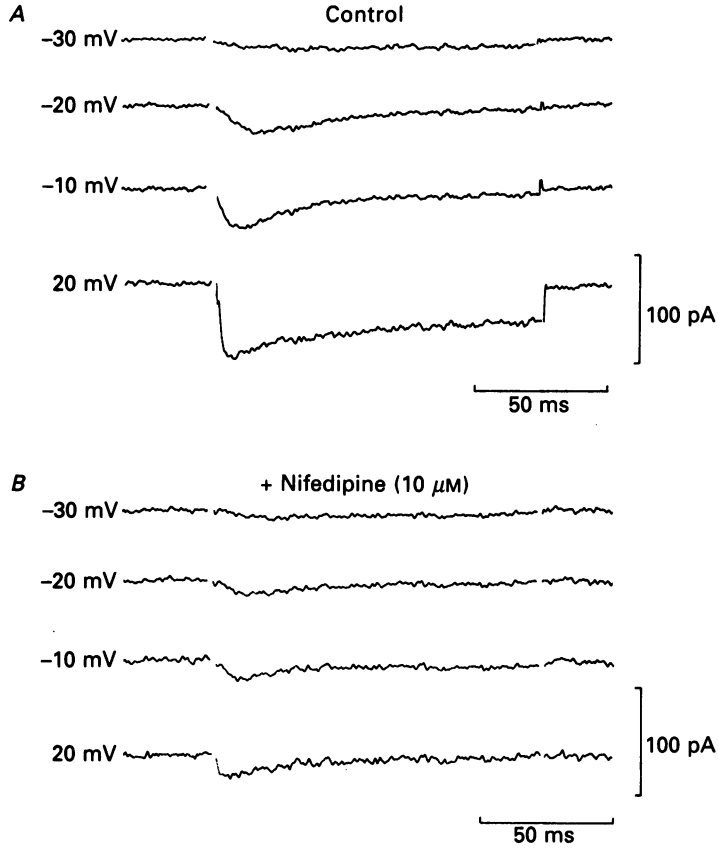

Fig. 12. Effect of nifedipine on Ca^{2+} current. *A*, control, produced by step depolarizations to potentials indicated on the left of traces (holding potential, -100 mV). *B*, effect of 10 μM-nifedipine.

Ensemble noise analysis

We employed the ensemble noise analysis technique (Neher & Stevens, 1977) to gain an initial estimate of the single-channel current amplitude. One important factor that can affect the estimation of single-channel current by the ensemble procedure is a change in the total number of channels during the course of the experiment. Possible contamination of the measurements by this factor were checked by comparing the current amplitudes acquired at various times during the ensemble analysis with the first few traces at the beginning of the ensemble. Current traces showing greater than 5% decline in their amplitude were not included in the analysis. Therefore errors in single-channel current measurements imposed by a change in the total fraction of activated channels was assumed to be negligible.

Figure 13 shows the averaged Ba^{2+} current records obtained from seventy-five current traces (Fig. 13*A*), and the estimated variance (Fig. 13*B*). The time-dependent decline in the variance paralleled that of the mean Ba^{2+} current, and the decline of both the parameters presumably reflects the slow decline in the current, attributable to the slow inactivation of the Ca^{2+} channels. The isochronal σ^2/I values

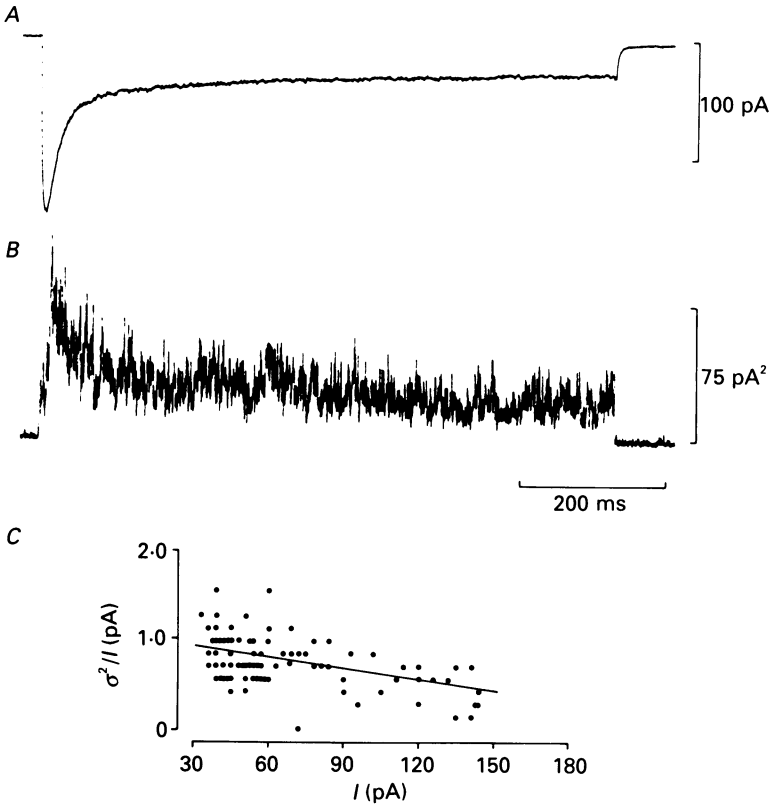

Fig. 13. Ensemble fluctuation variance in 50 mM-Ba^{2+}. *A*, mean Ba^{2+} inward current (I), average of seventy-five sweeps. *B*, variance (σ^2) at -10 mV. *C*, isochronal σ^2/I–I plot from the data shown in *A* and *B*. The straight line was drawn according to the linear regression equation, $1{\cdot}03 - 0{\cdot}0044\ I$, which gave a single-channel current amplitude of 1·03 pA and total number of channels, $N = 2500$. Filter frequency, 2 kHz; digitizing frequency, 4 kHz.

were plotted as a function of the mean current (I) in Cartesian co-ordinates, to estimate the single-channel current amplitude. The scatter plot was fitted by a linear regression equation and from the intercept of the straight line on the y-axis, a single-channel current amplitude of about 1 pA was estimated at the membrane potential of -10 mV and external Ba^{2+} concentration of 50 mM used in the experiment illustrated.

Single-channel currents

Outside-out patches containing single Ca^{2+} channels were obtained by withdrawing the electrode from the cell, after achieving access to the cell interior in the whole-cell recording configuration. Inward unitary currents were evoked during a voltage step

to −10 mV from a holding potential of −100 mV (Fig. 14). The probability of occurrence of channel opening appears to be random during the duration of the voltage step. It is more likely that the unitary inward channel current events shown reflect the unitary properties of the whole-cell Ca^{2+} current and in particular the properties of the Ca^{2+} channel type with slow inactivation characteristics. The

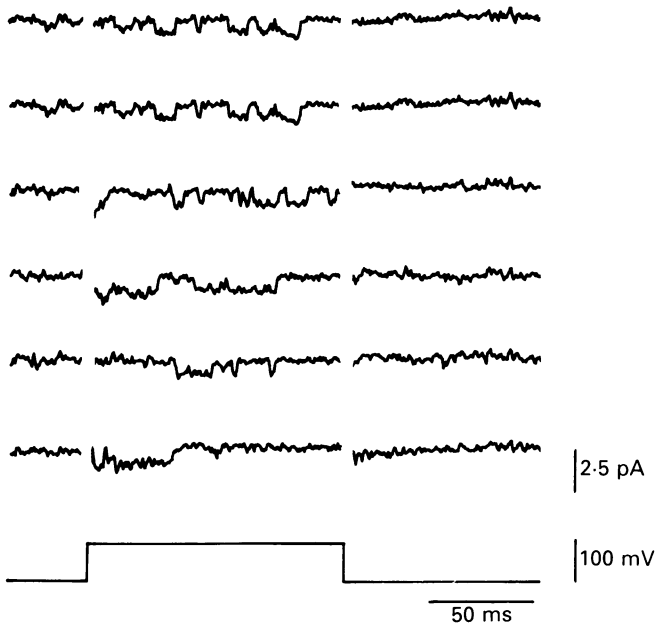

Fig. 14. Outside-out patch clamp records of voltage activated single-channel currents recorded in 50 mM-external Ba^{2+}. Filter frequency, 1 kHz; digitizing frequency, 2 kHz.

unitary inward current events can be further related to the L-channel type reported by Carbone & Lux (1984) and Nowycky, Fox & Tsien (1985). In other outside-out patch clamp recordings, we observed single-channel current events corresponding to the T-channel type (Nowycky *et al.* 1985), using depolarizing steps below −30 mV. In these, the occurrences of single-channel events were concentrated towards the beginning of the voltage step. The single-channel current amplitude of 1 pA corroborates with the single-channel current amplitude estimated from ensemble analysis (Fig. 13).

DISCUSSION

In this study we have investigated some of the properties and kinetic features of Ca^{2+} currents in gonadotrophs isolated from the sheep pars tuberalis. The currents were qualitatively similar to those reported in other pituitary cells in certain basic properties.

The discussion below is directed at relating some of the kinetic features of the voltage-dependent macroscopic Ca^{2+}/Ba^{2+} currents of these cells to hormone secretion. The possible differential contributory role of the current flow through the two channel types constituting the macroscopic divalent current in gonadotrophin

secretion is also considered. Another aspect discussed is whether the inactivation of the current is a Ca^{2+}-dependent or a Ca^{2+}-independent voltage-dependent process. In addition, comparisons of certain features with Ca^{2+} channel properties of other cell systems have been made.

Are Ca^{2+} channels in gonadotrophs regulated by intracellular Ca^{2+} or by voltage?

The mechanism of Ca^{2+} current inactivation in gonadotrophs can be attributed to a true decline in the inward current and not to activation of a simultaneous outward current, since the tail current amplitude showed a progressive decline paralleling the inactivation phase (Fig. 5).

The steady-state inactivation curve, determined using a two-pulse protocol (Fig. 6*B*), shows that conditioning pulse steps depressed the Ca^{2+} current generated by the test potential only at conditioning pulse potentials that evoked detectable inward currents. On the one hand, this indicates that the influx of divalent cations occurring during a pre-pulse volley depresses the subsequent current evoked by the test pulse (Eckert & Chad, 1984), but it is nevertheless possible to argue that the inactivation of Ca^{2+} current in the gonadotrophs is not dependent on the level of intracellular Ca^{2+}. For instance, the decreased test current amplitudes due to a pre-pulse were studied with Ba^{2+} as the external divalent cation and the results were similar with Ca^{2+} in the extracellular solution. Furthermore, all experiments with external Ca^{2+} or Ba^{2+} were performed in the presence of the Ca^{2+} chelator EGTA in the pipette solution used for dialysis. The absence of a U-shaped $h(\infty)$–V curve further substantiates the operation of voltage-dependent channel inactivation (Fox, 1981; Hadley & Hume, 1987).

A slight rightward shift of the maximal peak current along the voltage axis was observed at higher Ba^{2+} concentrations (Fig. 1*B*). Similar shifts of the peak current in the I–V relation have been observed before in rat clonal pituitary cells (Hagiwara & Ohmori, 1982) and have been attributed to the addition of positive charge to the external surface of the membrane by a higher concentration of Ba^{2+}, making the surface membrane potential more positive.

The voltage-dependent inactivation however, is not due to a shift in the electrochemical potential resulting from accumulation of internal Ca^{2+} or Ba^{2+} ions during the current flow. If this were true, steady-state inactivation with faster kinetics would be seen with Ba^{2+} current than with Ca^{2+} current, since Ba^{2+} current is larger than Ca^{2+} current, and both are activated at a similar rate. Further, a visual comparison of the Ba^{2+} current decay at two different external Ba^{2+} concentrations (Fig. 1*A*) shows that although the peak current amplitude was larger at higher Ba^{2+} concentration, no significant change in decline of the current was noticeable. Results similar to that shown in Fig. 1*A* were obtained, with Ca^{2+} as the external divalent cation.

For similar reasons it is difficult to ascribe the inactivation to depletion of Ba^{2+}/Ca^{2+} from an unstirred area around the membrane in the extracellular compartment. A change in the surface charge of the external membrane surface as a cause of inactivation is also unlikely; addition of more positive charge to the external surface would be expected to make the surface membrane potential more positive.

Two types of Ca^{2+} channels in gonadotrophs

Our results suggest the presence of two types of Ca^{2+} channels in the gonadotrophs. A shoulder on the *I–V* relationship of Ca^{2+}/Ba^{2+} currents indicative of two channel types reported in other cell types (e.g. De Reimer & Sakmann, 1986) was, however, not seen in the gonadotrophs. The activation phases of the Ca^{2+}/Ba^{2+} currents at the more depolarized potential range were fitted by a double-exponential function. Similarly, the inactivation phases of the Ca^{2+}/Ba^{2+} currents were fitted by a single-exponential function at less depolarized potentials and by a double-exponential function at more depolarized potentials (Fig. 7). Although the double-exponential fit might be argued to comprise two components of a single-channel type, additional evidence, however, indicated it to be otherwise.

The power spectral density plots were fitted by double, rather than single Lorentzian functions. This contrasts with single Lorentzian fits of Ba^{2+} current noise reported in the neoplastic pituitary GH3 cells (Hagiwara & Ohmori, 1982) and in snail neurones (Krishtal, Pidoplichko & Shakhovalov, 1981; Lux & Nagy, 1981). The time constant values closely approximated the relative values of the two components derived from exponential fits of the activation and inactivation portions of the current, and therefore probably reflect the inherent kinetics of the two different components contributing to the noise. This corroborates with findings reported for the adrenal chromaffin cells (Fenwick, Marty & Neher, 1982). In contrast to similar currents in lactotrophs (Cobbett *et al.* 1987), however, we found the two time constants to exhibit a degree of voltage dependence illustrated in Fig. 8, and appearance of the two channel types was voltage dependent. The fast inactivating component appeared on using depolarizing voltage steps from a more negative holding potential of -100 mV, and it disappeared at a less negative holding potential of -50 mV (Fig. 10).

A differential sensitivity of the two channel types to clamp frequency also supported the presence of two Ca^{2+} channel types in the gonadotrophs. A preferential attenuation of the fast inactivating component at higher clamp frequencies was a characteristic feature in these cells, without significant diminution of the slow inactivating current.

Differential pharmacological sensitivity of the two currents was also observed. Nifedipine strongly depressed the slow inactivating current, but was virtually without effect on fast inactivating component. A differential metabolic sensitivity of the two channel types was an additional observation. The slow inactivating component of Ca^{2+} current was consistently observed to run-down in the absence of ATP or cyclic AMP in the pipettes (Fedulova, Kostyuk & Vesolovsky, 1985; Cobbett *et al.* 1987), while their appearance was a normal feature with inclusion of the phosphorylating agents in the internal dialysate. This provided further support for the existence of two distinct populations of Ca^{2+} channel types.

The characteristics of activation voltage, inactivation kinetics and pharmacological sensitivity of the two populations of Ca^{2+} channels described for the gonadotrophs here are similar to the ones described in normal pituitary lactotrophs (De Reimer & Sakmann, 1986; Cobbett *et al.* 1987), smooth muscle cells (Friedman, Suarez-Kurtz, Kaczorowski, Katz & Reuben, 1986), dorsal root ganglion cells (Fedulova *et al.* 1985) and ventricular myocytes (Mitra & Morad, 1986).

Single-channel current amplitude

Ensemble noise analysis and outside-out patch-clamp recordings yielded single Ba^{2+} channel current amplitudes of about 1 pA. Since Ba^{2+} is twice as permeable as Ca^{2+} through Ca^{2+} channels and current amplitudes in external Ba^{2+} are doubled, the amplitude of single-channel current is probably about half of Ba^{2+} current, i.e. 0·5 pA. This value is large compared to that reported for other membrane systems (Krishtal *et al.* 1981; Hagiwara & Ohmori, 1982, 1983; Cobbett *et al.* 1987) but closely corresponds to the single-channel current value in Helix neurones (Lux & Nagy, 1981) and bovine adrenal chromaffin cells (Fenwick *et al.* 1982).

Functional significance of voltage-gated Ca^{2+} channels in luteinizing hormone (LH) secretion

An important question related to LH secretion is whether voltage-activated Ca^{2+} channels play a functional role in hormone release. In previous work on voltage-activated Na^+ currents in gonadotrophs (Mason & Sikdar, 1988), it was concluded that the role of Na^+ channels in LH secretion was probably vestigial, since incubating cells with TTX did not affect basal or GnRH-stimulated LH release. However, the importance of external Ca^{2+} entry into the cell for LH release was underlined by the observation of attenuated basal and GnRH-stimulated LH release in the presence of cobalt, a known blocker of voltage-activated Ca^{2+} channels.

From the steady-state inactivation curve (Fig. 6*B*), it is evident that 93% of Ca^{2+} channels are in an activatable state at a resting membrane potential of -70 mV recorded for these cells (Mason & Waring, 1985). By analysing the Ca^{2+} currents to depolarizing pulses from two different holding potentials, it was possible to separate the two components of Ca^{2+} current. From the activation curve of the Ca^{2+} current type with fast inactivation kinetics obtained by a subtraction procedure (Fig. 10*B*), it can be seen that at a membrane potential of -70 mV the amount of Ca^{2+} entry through this channel type is 8% of the maximal current evoked. Therefore, the small leak through the low-threshold Ca^{2+} channel with fast inactivation kinetics almost certainly contributes to a small resting influx of Ca^{2+} and might thus affect basal Ca^{2+} levels and release of hormone under resting conditions. Since a membrane potential of -70 mV would lie on a steep portion of the *I–V* curve, these data would also imply that a small depolarization induced by GnRH or the occurrence of GnRH-induced membrane fluctuations of ± 5–10 mV (Mason & Waring, 1985) could increase in a profound manner the amount of Ca^{2+} influx through this channel type and thereby promote increased LH release. The high-threshold Ca^{2+} channel type with slow inactivation kinetics might be thought to contribute more significantly to Ca^{2+} entry in situations where the membrane is depolarized beyond -40 mV, by KCl for instance (Mason & Waring, 1985).

The importance of voltage-activated Ca^{2+} channels in the physiological responsiveness of gonadotrophs to GnRH has recently been demonstrated by Shangold, Murphy & Miller (1988). Application of GnRH to single identified gonadotrophs induced an initial rapid rise of intracellular Ca^{2+} and then a fall to basal levels, followed by a secondary extended rise and fall. The secondary rise in intracellular Ca^{2+} was attributed to Ca^{2+} influx through L-type Ca^{2+} channels, since the secondary peak could be blocked by the dihydropyridine Ca^{2+} channel blocker, nitrendipine. As

a corollary to this recent observation, LH release has been shown to be dependent on Ca^{2+} influx through L-type channels. Nifedipine was found to suppress the slow sustained LH release phase but not the initial rapid LH release (Smith, Wakefield, King, Naor, Millar & Davidson, 1987). Suppression of the calcium current with slow kinetics in the ovine gonadotrophs could be related to these observations.

We wish to thank Miss A. L. V. Tibbs for her excellent technical help with cell culture and Mr Richard Bunting for preparing the illustrations. We are indebted to David Brown of the Statistics and Computing group, for his considerable help and time with modelling some of the equations that appear in the text. Dr Sikdar was supported by a Lalor Foundation Research Fellowship (USA).

REFERENCES

AKAIKE, N., LEE, K. S. & BROWN, A. M. (1978). The calcium current of *Helix* neuron. *Journal of General Physiology* **71**, 509–531.

BELLUZZI, O., SACCHI, O. & WANKE, E. (1985). Identification of delayed potassium and calcium currents in the rat sympathetic neurone under voltage clamp. *Journal of Physiology* **358**, 109–129.

BROWN, A. M., TSUDA, Y. & WILSON, D. L. (1983). A description of activation and conduction in calcium channels based on tail and turn-on current measurements in the snail. *Journal of Physiology* **344**, 549–583.

CARBONE, E. & LUX, H. D. (1984). A low voltage-activated, fully inactivating Ca channel in vertebrate sensory neurones. *Nature* **310**, 501–502.

COBBETT, P., INGRAM, C. D. & MASON, W. T. (1987). Voltage-activated currents through calcium channels in normal bovine lactotrophs. *Neuroscience* **23**, 661–677.

CONN, P. M., ROGERS, D. C. & SEAY, S. G. (1983). Structure–function relationship of calcium ion channel antagonists at the pituitary gonadotrope. *Endocrinology* **113**, 1592–1595.

DE RIEMER, S. A. & SAKMANN, B. (1986). Two calcium currents in normal rat anterior pituitary cells identified by a plaque assay. In *Calcium Electrogenesis and Neuronal Functioning*, ed. HEINEMANN, U., KLEE, M., NEHER, E. & SINGER, W., pp. 139–154. Berlin, Heidelberg: Springer–Verlag.

DUBINSKY, J. M. & OXFORD, G. S. (1984). Ionic currents in two strains of rat anterior pituitary tumor cells. *Journal of General Physiology* **83**, 309–339.

ECKERT, R. & CHAD, J. E. (1984). Inactivation of Ca channels. *Progress in Biophysics and Molecular Biology* **44**, 215–267.

FEDULOVA, S. A., KOSTYUK, P. G. & VESELOVSKY, N. S. (1985). Two types of calcium channels in the somatic membrane of new-born rat dorsal root ganglion neurones. *Journal of Physiology* **359**, 431–446.

FENWICK, E. M., MARTY, A. & NEHER, E. (1982). Sodium and calcium channels in bovine chromaffin cells. *Journal of Physiology* **331**, 599–635.

FOX, A. P. (1981). Voltage-dependent inactivation of a Ca-channel. *Proceedings of the National Academy of Sciences of the USA* **78**, 953–956.

FRIEDMAN, M. E., SUAREZ-KURTZ, G., KACZOROWSKI, G. J., KATZ, G. M. & REUBEN, J. P. (1986). Two calcium currents in a smooth muscle cell line. *American Journal of Physiology* **250**, H699–703.

GROSS, D. S., TURGEON, J. L. & WARING, D. W. (1984). The ovine pars tuberalis: a naturally occurring source of partially purified gonadotropes which secrete luteinizing hormone *in vitro*. *Endocrinology* **114**, 2084–2091.

HADLEY, R. W. & HUME, J. R. (1987). An intrinsic potential-dependent inactivation mechanism associated with calcium channels in guinea-pig myocytes. *Journal of Physiology* **389**, 205–222.

HAGIWARA, S. & BYERLY, L. (1981). Calcium channel. *Annual Review of Neuroscience* **4**, 69–125.

HAGIWARA, S., MIYAZAKI, S., MOODY, W. & PATLAK, J. (1978). Blocking effects of barium and hydrogen ions on the potassium current during anomalous rectification in the starfish egg. *Journal of Physiology* **279**, 167–185.

HAGIWARA, S. & OHMORI, H. (1982). Studies of calcium channels in rat clonal pituitary cells with patch electrode voltage clamp. *Journal of Physiology* **331**, 231–252.

HAGIWARA, S. & OHMORI, H. (1983). Studies of single calcium channel currents in rat clonal pituitary cells. *Journal of Physiology* **336**, 649–661.

HODGKIN, A. L. & HUXLEY, A. F. (1952). A quantitative description of membrane current and its application to conduction and excitation in nerve. *Journal of Physiology* **117**, 500–544.

KOSTYUK, P. G., VESELOVSKY, N. S. & FEDULOVA, S. A. (1981). Ionic currents in the somatic membrane of rat dorsal root ganglion neurons. II. Calcium currents. *Neuroscience* **6**, 2431–2437.

KRISHTAL, O. A., PIDOPLICHKO, V. I. & SAKHOVALOV, YU. A. (1981). Conductance of the calcium channel in the membrane of snail neurones. *Journal of Physiology* **310**, 423–434.

LLINÁS, R., STEINBERG, I. Z. & WALTON, K. (1981). Presynaptic calcium currents in squid giant synapse. *Biophysical Journal* **33**, 289–321.

LUX, H. D. & NAGY, K. (1981). Single channel Ca^{2+} currents in *Helix pomatia* neurons. *Pflügers Archiv* **391**, 252–254.

MASON, W. T. & RAWLINGS, S. R. (1988). Whole-cell recordings of ionic currents in bovine somatotrophs and their involvement in growth hormone secretion. *Journal of Physiology* **405**, 577–593.

MASON, W. T. & SIKDAR, S. K. (1988). Characterization of voltage-gated sodium channels in ovine gonadotrophs: relationship to hormone secretion. *Journal of Physiology* **399**, 493–517.

MASON, W. T., SIKDAR, S. K. & WARING, D. W. (1986). Voltage-dependent ionic currents in normal gonadotrophs of the ovine pars tuberalis. *Journal of Physiology* **376**, 26*P*.

MASON, W. T. & WARING, D. W. (1985). Electrophysiological recordings from gonadotrophs. Evidence for Ca^{2+} channels mediated by gonadotrophin-releasing hormone. *Neuroendocrinology* **41**, 258–268.

MASON, W. T. & WARING, D. W. (1986). Patch-clamp recordings of single ion channel activation by gonadotrophin-releasing hormone in ovine pituitary gonadotrophs. *Neuroendocrinology* **43**, 205–219.

MATTESON, D. R. & ARMSTRONG, C. M. (1984). Na and Ca channels in a transformed line of anterior pituitary cells. *Journal of General Physiology* **83**, 371–394.

MENTRARD, D., VASSORT, G. & FISCHMEISTER, R. (1984). Calcium-mediated inactivation of the calcium conductance in cesium-loaded frog heart cells. *Journal of General Physiology* **83**, 105–131.

MITRA, R. & MORAD, M. (1986). Two types of calcium channels in guinea pig ventricular myocytes. *Proceedings of the National Academy of Sciences of the USA* **83**, 5340–5344.

NEHER, E. & STEVENS, C. F. (1977). Conductance fluctuations and ionic pores in membranes. *Annual Review of Biophysics and Bioengineering* **6**, 345–381.

NOWYCKY, M. C., FOX, A. P. & TSIEN, R. W. (1985). Three types of neuronal calcium channels with different calcium agonist sensitivity. *Nature* **316**, 440–443.

OKAMOTO, H., TAKAHASHI, K. & YOSHII, M. (1976). Two components of the calcium current in the egg cell membrane of the tunicate. *Journal of Physiology* **255**, 527–561.

QUANDT, F. N. & NARAHASHI, T. (1984). Isolation and analysis of inward currents in neuroblastoma cells. *Neuroscience* **13**, 249–262.

SHANGOLD, G. A., MURPHY, S. N. & MILLER, R. J. (1988). Gonadotropin-releasing hormone-induced Ca^{2+} transients in single identified gonadotropes require both intracellular Ca^{2+} mobilization and Ca^{2+} influx. *Proceedings of the National Academy of Sciences of the USA* **85**, 6566–6570.

SMITH, C. E., WAKEFIELD, I., KING, J. A., NAOR, Z., MILLAR, R. P. & DAVIDSON, J. S. (1987). The initial phase of GnRH-stimulated LH release from pituitary cells is independent of calcium entry through voltage-gated channels. *FEBS Letters* **225**, 247–250.